Article

Ultrasound-Responsive Micelle-Encapsulated Mesenchymal Stem Cell-Derived EVs for the Treatment of Lower Limb Microcirculation Disease

Peng Guo, Qian Wang, Ling Chen, Kun Dingya, and Bing Wang*

Read Online

ACCESS | Metrics & More | Article Recommendations | SI Supporting Information

ABSTRACT: Lower limb microcirculatory ischemic disease is a vascular disorder primarily characterized by limb pain, gangrene, and potential amputation. It can be caused by various factors, such as hyperglycemia, atherosclerosis, and infection. Due to the extremely narrow luminal diameter in lower limb microcirculatory ischemic lesions, both surgical and medical interventions face challenges in achieving satisfactory therapeutic outcomes within the microvessels. Extracellular vesicles derived from mesenchymal stem cells (MSCs-EVs) exhibit promising potential in the treatment of microcirculation ischemic lesions due to their small size and ability to promote angiogenesis. After undergoing substantial losses during the process of EVs transportation, only a minimal fraction of EVs can effectively reach the site of microcirculatory lesions, thereby compromising the therapeutic efficacy for microcirculatory disorders. Herein, an ultrasound-responsive system utilizing 2-(dimethylamino)ethyl methacrylate-b-2-tetrahydropyranyl methacrylate (DMAEMA-b-THPMA) micelles to encapsulate MSCs-EVs has been successfully constructed, with the aim of achieving localized and targeted release of EVs at the site of microcirculatory lesions. The reversible addition−fragmentation chain transfer (RAFT) polymerization method facilitates the successful synthesis of diblock copolymers comprising monomer 2-(dimethylamino)ethyl methacrylate (DMAEMA) and monomer 2-tetrahydropyranyl methacrylate (THPMA). The DMAEMA-b-THPMA micelles exhibit a nanoscale structure, reliable biocompatibility, ultrasound responsiveness, and conspicuous protection of EVs. Furthermore, the implementation of low-energy-density ultrasound can enhance angiogenesis by upregulating the levels of the vascular endothelial growth factor (VEGF). In in vivo experiments, the ultrasound-responsive system of the DMAEMA-b-THPMA micelles and MSCs-EVs synergistically enhances therapeutic efficacy by promoting angiogenesis, improving vascular permeability, and optimizing vascular. In conclusion, this work demonstrates bioapplication of an ultrasound-responsive micellar nanosystem loaded with EVs for the treatment of lower limb microcirculatory ischemic disorders.
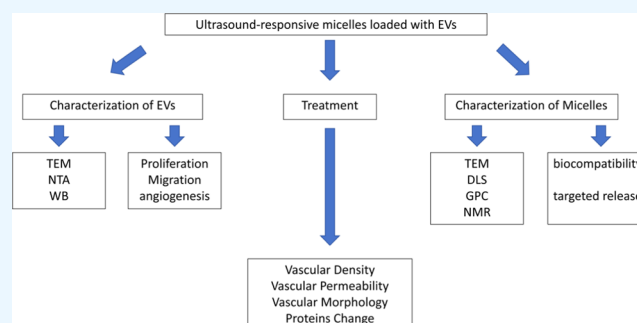
INTRODUCTION

Arteriosclerotic occlusive disease or diabetic complications often lead to lower limb ischemia in individuals diagnosed with peripheral artery disease (PAD). Patients with severe lower limb ischemia also develop adverse outcomes, such as limb gangrene and amputation.[1] To date, surgical treatments and endovascular interventional therapies are the main treatment strategies for lower limb ischemic diseases.[2] Nevertheless, surgical interventions pose significant dangers for older individuals with preexisting conditions and are limited in their ability to treat peripheral microcirculation lesions.[3] On the other hand, conservative medication primarily serves to slow the progression of lower limb ischemic diseases. Preventative treatment is not effective for patients with severe lesions.[4]

With the advancement of regenerative medicine, the use of stem cell implantation therapy has become a feasible approach for treating different diseases.[5] In the management of lower

limb ischemic diseases,[6] stem cell transplantation has also demonstrated a favorable therapeutic outcome. Various methods are used in stem cell transplantation therapy to primarily treat diseases related to insufficient blood flow in lower limbs. Initially, stem cells possess the capacity to transform into various types of cells such as endothelial cells and smooth muscle cells. The transplantation of stem cells has the ability to transform into vascular endothelial cells and enhance the development and restoration of fresh blood vessels, consequently enhancing the state of lower limb ischemia.[7] Furthermore, implanted stem cells can secrete
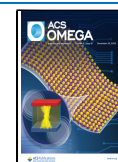
diverse growth factors and cytokines, including vascular endothelial growth factor (VEGF) and matrix metalloproteinases. These substances are capable of stimulating blood vessel development and facilitating the healing and rejuvenation of nearby tissues. Immunomodulation can enhance lower limb ischemia as well as stem cell transplantation. Stem cells can inhibit the inflammatory response by changing macrophage polarization and by reducing inflammatory cell infiltration in injured tissues.[8] There are, however, many obstacles to the clinical application of mesenchymal stem cell (MSCs) therapy, such as low homing efficiency,[9] stem cell immunogenicity,[10] and stem cell carcinogenicity.[11] The microvascular network is composed of capillaries and arterioles with diameters less than 100 μm, but stem cells range from micrometers to millimeters in diameter.[12] Therefore, it is difficult for stem cells to reach microcirculation lesions and exert therapeutic effects.[13] Therefore, it is crucial to discover a substitute for therapy involving the transplantation of stem cells.

The continuous and extensive examination of EVs has introduced fresh possibilities for addressing microcirculation lesions.[14] MSCs-EVs have sizes ranging from 40 to 150 nm, and they exhibit comparable biological effects to MSCs.[15] Moreover, compared with stem cell therapy, EVs treatment greatly reduces tumorigenicity.[16] Thus, MSCs-EVs have the ability to effectively substitute MSCs in the management of microcirculation diseases.[17] Our previous study showed that MSCs-EVs have satisfactory therapeutic effects against ischemic diseases.[18]

Nevertheless, when EVs are administered intravenously, they primarily accumulate in the heart, liver, spleen, and kidney, with only a minor fraction capable of affecting peripheral microvessels.[19] This not only impacts the healing effectiveness of EVs for treating microvascular conditions but also heightens the nonselective attachment of EVs to other organs. Hence, it is crucial to develop a nanosystem capable of precisely controlling the release of EVs to a specific location. Block polymers have been extensively utilized in drug delivery research in recent years.[20] Usually, a hydrophobic drug is encapsulated inside the micelle. When the micelles are subjected to specific stimuli, the structure changes and the internal drug is released. Ultrasound is a cost-effective, easy-to-use, versatile, and safe medical technology.[21] Ultrasound was used in this research to modify the configuration of DMAEMA-*b*-THPMA micelles with the aim of controlling the release of internally encapsulated EVs. Based on the distinctive attributes of MSCs-EVs and DMAEMA-*b*-THPMA micelles, a nanosystem that integrates ultrasound-responsive micelles with EVs was designed. Through the RAFT polymerization method, DMAEMA-*b*-THPMA copolymers with a nanoscale structure, reliable biocompatibility, and ultrasound responsiveness were prepared. In *in vivo* experiments, the combination of DMAEMA-*b*-THPMA micelles and EVs exhibited significant therapeutic efficacy in a murine model of lower limb microcirculatory ischemia. Overall, this work highlights the potential of ultrasound-responsive micelles loaded with EVs for treating microcirculatory ischemic diseases.

■ EXPERIMENTAL SECTION

Preparation and Characterization of THPMA. The synthesis of the THPMA monomer involved the addition reaction of methacrylic acid (MAA) with 3,4-dihydro-2H-pyran (DHP). The combination of 3,4-dihydro-2H-pyran (21.51 mL, 19.84 g, 0.2358 mol), methacrylic acid (10 mL, 10.15 g, 0.1179 mol), and p-toluenesulfonic acid monohydrate catalyst (TsOH) was placed in a round-bottom flask with two necks. The flask was equipped with a magnetic stirring bar and had a total capacity of 100 mL. The solution was agitated at a temperature of 70 °C for a duration of 24 h with a stirring rate of 300 rpm. Afterward, the blend underwent two passes through an alkaline alumina column to remove any remaining or excessive methacrylic acid along with other unwanted proton impurities that were present. To remove all moisture and residual acidic impurities completely from THPMA, it was stirred on CaH_2. Finally, the obtained THPMA product was stored in darkness at −20 °C to minimize the occurrence of self-polymerization. The THPMA synthesis method is consistent with the reported literature.[22]

Preparation and Characterization of DMAEMA-*b*-THPMA. The copolymerization of THPMA and DMAEMA was conducted via the RAFT polymerization method utilizing ethyl 2-bromoisobutyrate (EBrB) to synthesize a DMAEMA-*b*-THPMA copolymer. Initially, a 10 mL round-bottom flask was prepared by eliminating the obstructing agent. Then, the DMAEMA monomer (1.98 g, 12.6 mmol) and THPMA monomer (1.43 g, 8.4 mmol) were introduced. Next, a functional resolution was created by dissolving CuBr (0.0101 g, 0.07 mmol) and ERBR (0.0137 g, 0.07 mmol) in 2 mL of anisole. The flask received the implemented solution. Three freeze−pump−thaw cycles were used to eliminate air from the reaction system. The RAFT reaction was conducted at a temperature of 70 °C for 2 h under N_2. Upon completion of the reaction, it was immediately quenched by being transferred to a Dewar flask containing liquid nitrogen to halt further RAFT polymerization. Finally, residual DMAEMA and THPMA were separated and removed using an ice-cold diethyl ether solvent. This synthesis method is similar to other reported approaches for synthesizing polymers via RAFT.[23] The analysis of proton nuclear magnetic resonance (^{1}H NMR) was conducted by utilizing an EFT-90 nuclear magnetic resonance spectrometer (Anasazi). The gel permeation chromatography (GPC) test was performed with an Agilent LC1200 from the United States of America using THF as the mobile phase at a temperature of 25 °C, a flow rate of 1 mL/min, and a sample concentration of 1 mg/mL, and the sample's weight-averaged molecular weight (M_n), number-averaged molecules (M_w), and molecular weight distribution (PDI) were obtained by integrating the effluent curve. The dynamic light scattering test was conducted on a 90Plus zeta-type potentiometer (Brookhaven).

Isolation and Characterization of EVs. The SNC Life Bank supplied human umbilical cord mesenchymal stem cells (HUCMSCs). The HUCMSCs were subsequently incubated at 37 °C in DMEM/F12 medium (Gibco 11320033). Figure 2A shows a schematic diagram of how EVs are separated.[24] The HUCMSC medium was collected when the cell confluency reached 80−90%. After the mixture was spun at a force of 2000 times gravity for 10 min, the liquid portion was gathered to remove any remnants of cells. Following an additional centrifugation at a speed of 10,000 times the force of gravity for a duration of 20 min, any remaining cellular debris was eliminated. After passing through a Millipore 0.22 μm filter, the liquid above the sediment was filtered. Next, following two rounds of centrifugation at a speed of 100,000*g* for a duration of 70 min, the sediment was gathered to acquire the EVs, which were subsequently subjected to

additional purification. After EVs were isolated from cell culture, they were suspended in PBS and then stored at −80 °C for future experiments.

The shapes and ultrastructures of the EVs were observed with transmission electron microscopy.[25] The EVs were fixed with 2.5% glutaraldehyde before imaging. For the subsequent procedure, 10 μL of this mixture was placed onto a copper grid and left to dry for 10 min in direct sunlight. Following a 10 min interval, the cells were stained with 2% phosphotungstic acid for counterstaining. A Zeiss Libra 120 transmission electron microscope was used to capture TEM images at 120 kV. The diameter distribution of EVs was detected by nanoparticle tracking assay (NTA).[26] 5 μL of EVs was diluted with methanol to 1.0 mL, and a pipet was used to carefully aspirate and mix the solution. Prior to analysis, samples were transferred to a sample pool. The parameters were set as follows: particle size range, 50−200 nm; molecular weight range 1000−220107 Da; temperature range 25 °C; laser 4.0 mW He−Ne; and wavelength 633 nm. Each sample was analyzed three times in a row. The data were analyzed by NanoSight NTA data analysis software. CD9, CD63, and CD8140, which are specific biomarkers for EVs, were identified through Western blot analysis.[27] EVs protein concentrations were measured using a BCA assay kit (Thermo Fisher, 23250).

Extracted EVs were labeled using a DIO fluorescent dye kit (Biyuntian, model C1993S) to assess their *in vitro* release. The discolored EVs solution was combined with a micelle solution of DMAEMA-*b*-THPMA in a proportion of 1−5. The remedy was magnetically stirred at 40 °C for a duration of 2 h. The combined mixture was then inserted into a dialysis membrane for the purpose of dialysis. After 24 h of dialysis, the liquid surface was subjected to a 1.5 W/cm^2 ultrasound. The dispersion of EVs before and after ultrasound was observed by confocal microscopy (Zeiss, Germany). To assess EVs release from micelles under various ultrasound conditions, micelles loaded with EVs were subjected to ultrasound at varying energy intensities and durations. To evaluate the level of EVs release under different energy intensities and durations of ultrasound action,[28] the BCA protein quantification technique was utilized to measure the concentration of released EVs.

In Vivo Release of EVs. For the *in vivo* study, mice of approximately identical age and weight belonging to the db/db strain were utilized. The extracted EVs were stained with a DiR fluorescent dye kit (Thermo Fisher, D12731). DiR-stained EVs (200 μL, 0.5 μg/μL) and DiR-stained EVs-loaded micelles (200 μL, 0.5 μg/μL) were injected into the caudal vein. Unilateral lower limbs of mice from both groups were treated with ultrasound for 20 min. The fluorescence intensity of organs *in vivo* was measured at 0.5 and 24 h using an *in vivo* imaging system (Berthold, LB983NC100, Germany).[29]

In Vitro Cytotoxicity Analysis. CCK-8 and live/dead cell staining[30] were utilized to observe the impact of micelles on umbilical vein endothelial cells. Endothelial cells from the umbilical vein of humans (HUVECs) were placed in 96-well plates with a seeding density of 1 × 10^4 cells per well. These cells were then cultured in DMEM in a volume of 100 μL per well supplemented with 10% FBS. PBS solution was added to the edges of the 96-well plates. Human umbilical vein endothelial cells (HUVECs) were cultured at 37 °C with 5% CO$_2$ for 24 h. Following a 24 h incubation period, the cells continued to adhere to the glass surface. Next, the medium was replaced with new medium and exposed to varying concentrations of DMAEMA-*b*-THPMA micelles for 24 h. Afterward, we introduced 10 μL of CCK-8 solution (Beyotime, C0038, China) to each well and incubated it at 37 °C for 2 h. Next, the absorbance was measured at a wavelength of 450 nm by utilizing a microplate reader specifically designed for absorbance readings (with a reference wavelength set at 650 nm). Furthermore, the viability of HUVECs was assessed using a live/dead viability/cytotoxicity kit following exposure to micelles at different concentrations. Immunofluorescence microscopy images were utilized to estimate live and dead cell counts in the same way.

In Vivo Cytotoxicity Analysis. Through the tail vein, micelles and PBS were administered to the mice at 24 weeks of age. The mice were euthanized by cervical dislocation after a 24 h period. HE staining was performed on heart, liver, spleen, lung, kidney, and tumor specimens.

EVs in HUVEC Proliferation. The impact of EVs on the growth of endothelial cells was assessed using CCK-8 and live/dead cell staining.[31] The experimental method aligned with the *in vivo* toxicity test procedure.

EVs Uptake Assay. The staining of EVs was performed by adding DiO (10 μM) and incubating the mixture at 4 °C for 30 min. Next, the suspension underwent centrifugation at 4 °C for 10 min at 4000g using an Amicon Ultra ultrafiltration tube (100 kDa) from Millipore, located in the USA. Afterward, the solution underwent sterile filtration using a 0.2 μm PES filter membrane and was subsequently stored at a temperature of 4 °C for future utilization. Human umbilical vein endothelial cells (HUVECs) were seeded at a density of 1 × 10^5 cells per well in a 24-well plate. The cells were cultured overnight in a 5% CO2 environment at 37 °C. Once the cells had attached to the wall, the HUVECs that had been seeded in 24-well plates were introduced into the monolayers along with the DiO-labeled EVs. The cells were treated with 4% formaldehyde in PBS after 4 h. Afterward, the cells underwent three rounds of washing in PBS. Afterward, additional rinses with PBS were conducted to eliminate formaldehyde. Next, the cells were stained with TRITC-conjugated phalloidin for 30 min. Following three rinses using PBS, the cell nuclei were stained with DAPI for a duration of 30 s. HUVECs[32] were observed for the uptake of EVs using confocal microscopy.

Cell Migration Assay. Cells were gathered and transferred to a suspension of individual cells during the exponential growth phase. Five hundred thousand cells were plated in each well of six-well plates, and the cells were cultured for 24 h. Once the cells achieved complete confluency, a line was marked across the layer of cells using a 1000 μL pipet tip. Floating cells were aspirated by pipet and washed with PBS. Culture medium (DMEM, 2% FBS) containing EVs was added to 6-well plates to culture cells. Images were taken under a microscope after 24 h of incubation. Using ImageJ software, the migration distance was calculated for the processed images.[33]

Tube Information Assay. A 96-well culture plate was precooled to 4 °C. All procedures were performed on ice to prevent the Matrigel from solidifying. To solidify, each well was supplemented with 50 μL of Matrigel and then placed in an incubator at 37 °C for a duration of 1 h. In each well, 3 × 10^4 cells were added and then incubated for 18 h in an incubator. Then, the number of tubules and the integrity of the tubule structure were observed under a microscope.[34]
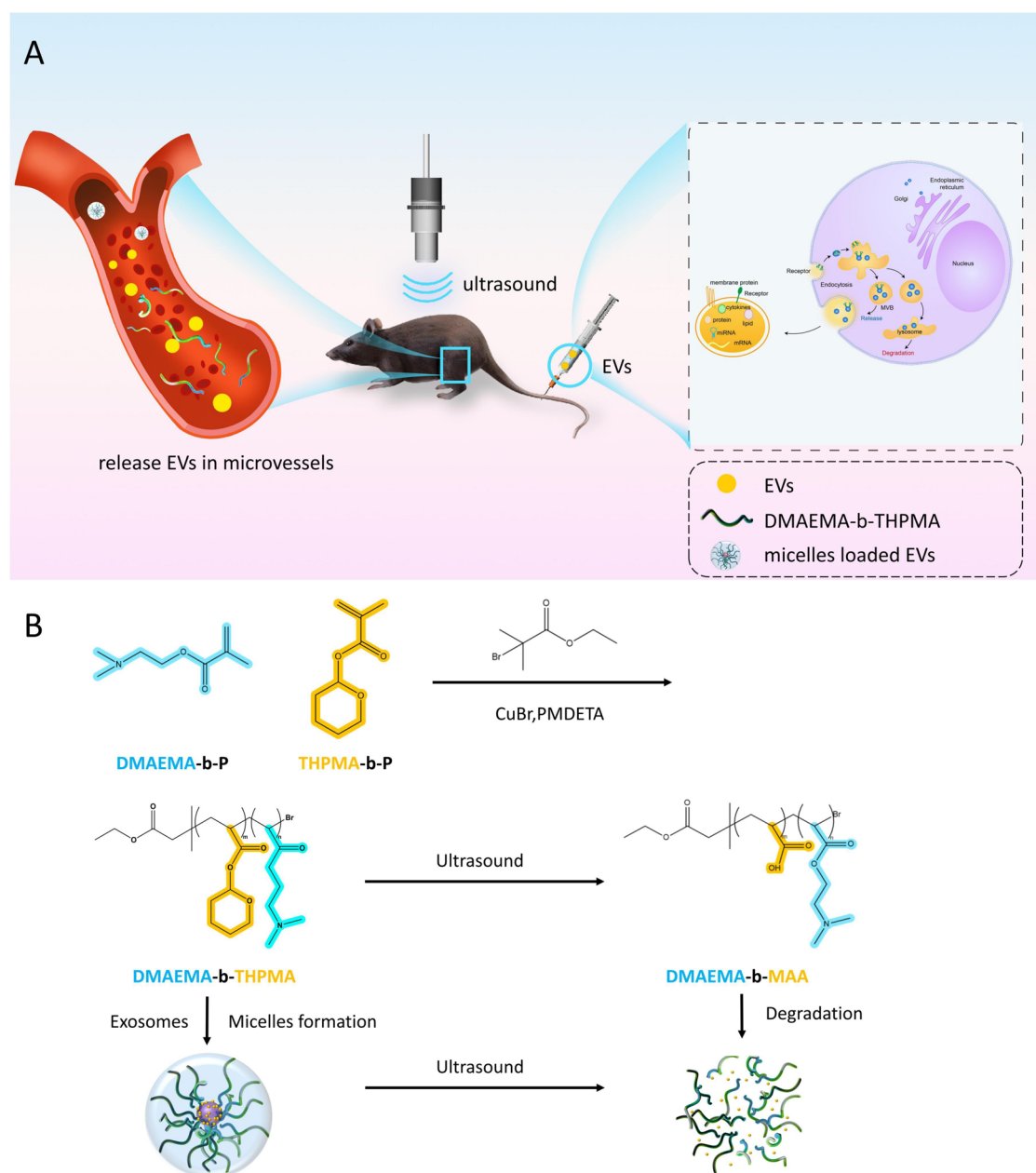
Figure 1. (A) Schematic of the targeted release of EVs from ultrasound-responsive micelle-loaded EVs in mice under ultrasound. (B) The THPMA monomer and DMAEMA monomer were copolymerized into DMAEMA-*b*-THPMA micelles using the RAFT polymerization method. Under the influence of ultrasound, ester bonds within micelles undergo cleavage, leading to the release of EVs encapsulated by the micelles.

Modeling Microcirculation Lesions in Mice. Male db/db mice, weighing between 34.3 and 39.7 g and aged 8 weeks, were acquired from Shanghai Model Organisms Center. Approval for the animal experimental protocol was granted by the Laboratory Animal Care and Ethics Committee of the Fifth Affiliated Hospital of Zhengzhou University (No. KY2022046). The mice were housed under conditions of 26 °C, 50% relative humidity, and a light/dark cycle of 12 h. Random blood glucose measurements were taken weekly. For a duration of 24 weeks, the mice were provided with a diet that was high in fat. The mice were categorized into the PBS group, micelle group, EVs group (50 μg), EVs group (100 μg), and micelle + EVs group (50 μg).

Permeability of Microcirculation by Evans Blue (EB) Perfusion. To evaluate the permeability of lower limb microvessels, EB staining was performed.[35] A dose of EB (0.5%, 1.5 mL/kg) was administered through the tail vein and allowed to circulate for 1 h. Following anesthesia using 30−40 mg/kg 1% sodium pentobarbital, the chest was opened, and a solution of heparin saline (0.9% sodium chloride +20 U/mL heparin sodium) was intracardially infused, totaling 200−300 mL. When the outflow from the right atrium became clear, perfusion was stopped, and the musculature of the lower limbs was extracted as quickly as possible. Dehydrated tissues were embedded in paraffin and cut into slices of 5 mm thickness. Following the washing of the slides, they were further treated with a DAPI working solution (100 g/mL) for 20 min at room temperature before undergoing another round of washing. EB dye permeation was observed by fluorescence microscopy.
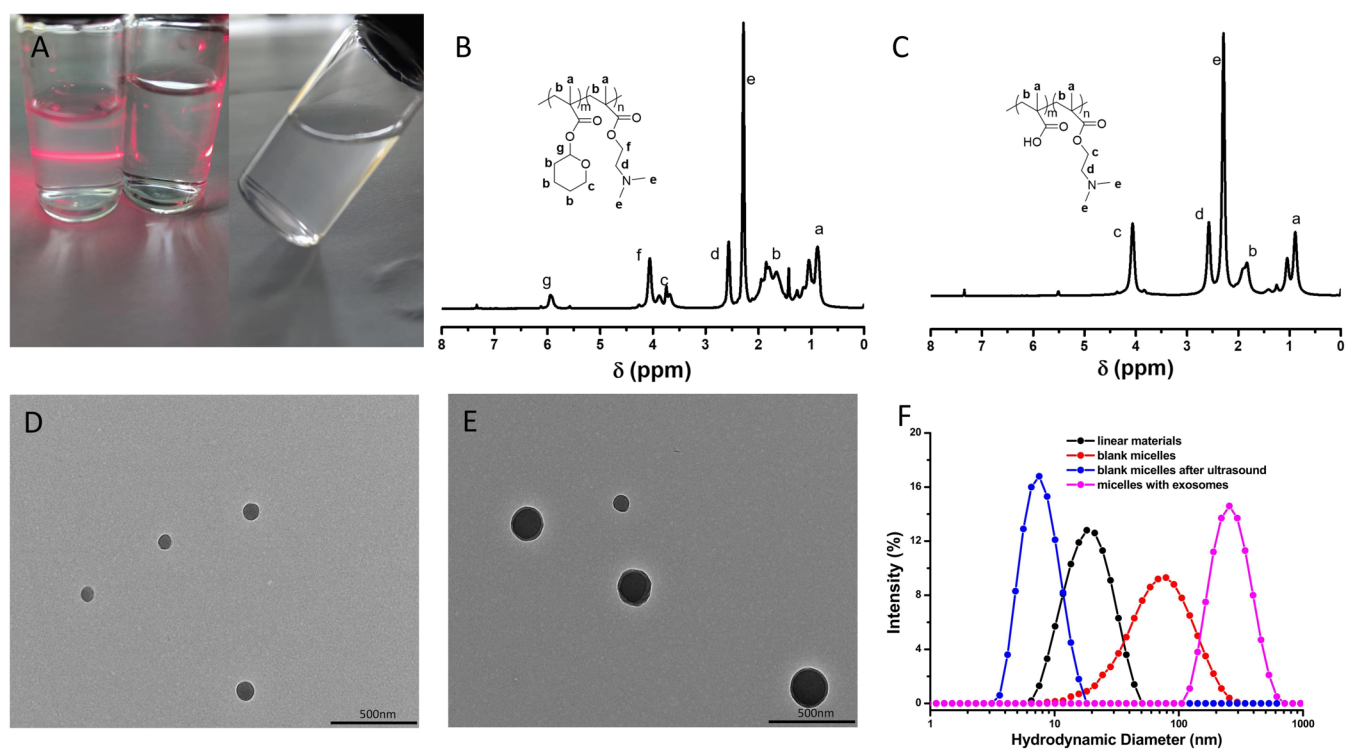
Figure 2. Characterization of micelles. (A) The Dingdall phenomenon of micelles. The left bottle contained the DMAEMA-*b*-THPMA micelle solution, and the right bottle contained the ethanol solution. The left bottle formed a light path under laser irradiation, while the right bottle did not. The micelles were observed as a colorless and transparent solution. (B) ¹H NMR spectrum of DMAEMA-*b*-THPMA. (C) ¹H NMR spectra of DMAEMA-*b*-MAA. (D) Electron microscopy of the DMAEMA-*b*-THPMA micelles (bar: 500 nm). (E) Electron microscopy of the EVs-loaded micelles (bar:500 nm). (F) Hydrodynamic radius of linear materials, blank micelles, blank micelles after ultrasound, and EVs-loaded micelles by DLS.

Immunofluorescence Analysis. To observe the angiogenic effects of EVs in mice with microcirculation lesions, CD31 immunofluorescence staining was performed on muscle tissue sections from the lower limbs.[36] Tissues were dehydrated with different concentrations of the ethanol solution, embedded in paraffin, sectioned at 7 μm, and dewaxed with xylene. Subsequently, the sections were heated in 0.01 mol/L EDTA buffer (pH 9.0) using a microwave for antigen retrieval. They were then placed at 37 °C for 10 min in the presence of 10% normal horse or goat serum to prevent the attachment of nonspecific immunoglobulins. The section was kept at a temperature of 4 °C overnight and incubated with a primary antibody (specifically, a mouse antihuman CD31 monoclonal antibody, 1200 dilution, ab222783 from Abcam). After being washed three times with PBS, the sections were incubated with the secondary antibody in the dark for 50 min, following the primary incubation. Afterward, the sections were incubated for 10 min with DAPI. As a final step, after 1% glycerin was sealed, tissue sections were observed by fluorescence microscopy.

Ultrastructure of Microcirculation under TEM. The lower limb tissues were obtained and trimmed from mice and fixed into 1 cm³ blocks at a low temperature in 2.5% glutaraldehyde. Afterward, the lower limb tissues of mice were fixed in a solution of 2.5% glutaraldehyde (pH 7.4) for a duration of 2 h, followed by immersion in 1% osmic acid for another 2 h at a temperature of 4 °C. Afterward, the specimens underwent three washes in 0.1 M phosphate buffer (pH 7.2).

To dehydrate the tissues, an ethanol gradient was applied, followed by 15 min of incubation in 100% acetone. The larvae

were subjected to treatment with acetone 812 embedding agent for 1 h, followed by treatment with 812 embedding agent for 1 h. Subsequently, they were incubated at a temperature of 60 °C for 4 h to facilitate the polymerization of the embedding resin. Ultrathin sections (70 nm) were stained by using uranyl acetate and lead citrate. After drying, the sample was observed under TEM.[37]

Analysis Using the Western Blot Technique. The protein expression levels of Bax, Bcl-2, and vegf-α[38] were analyzed using Western blotting. Saline perfusion was performed on the muscle tissue of the lower limbs, and blood clots were immediately washed away with 0.9% normal saline (4 °C). Sections of muscle tissue from each group were cut into 1 mm blocks. The muscle tissue was homogenized with a reagent for extracting the tissue protein. The liquid above the sediment was obtained by spinning at a force of 10,000 times the acceleration due to gravity for a duration of 10 min at a temperature of 4 °C. Extraction of protein was performed by adding equal volumes of loading buffer (2× SDS) to each sample. Five min of boiling in a water bath denatured the samples. Afterward, separation gels with a concentration of 10% and a concentration gel of 4% were made. Subsequently, the SDS/polyacrylamide gel was placed in an electrophoresis tank for loading and conducting electrophoresis. After 20 and 80 min of electrophoresis, the samples were dried at 70 and 110 V, respectively. Next, the proteins were transferred to PVDF membranes. Following blocking of the membranes, incubation was carried out using various primary antibodies, followed by incubation with secondary antibodies. Next, the membranes underwent another round of
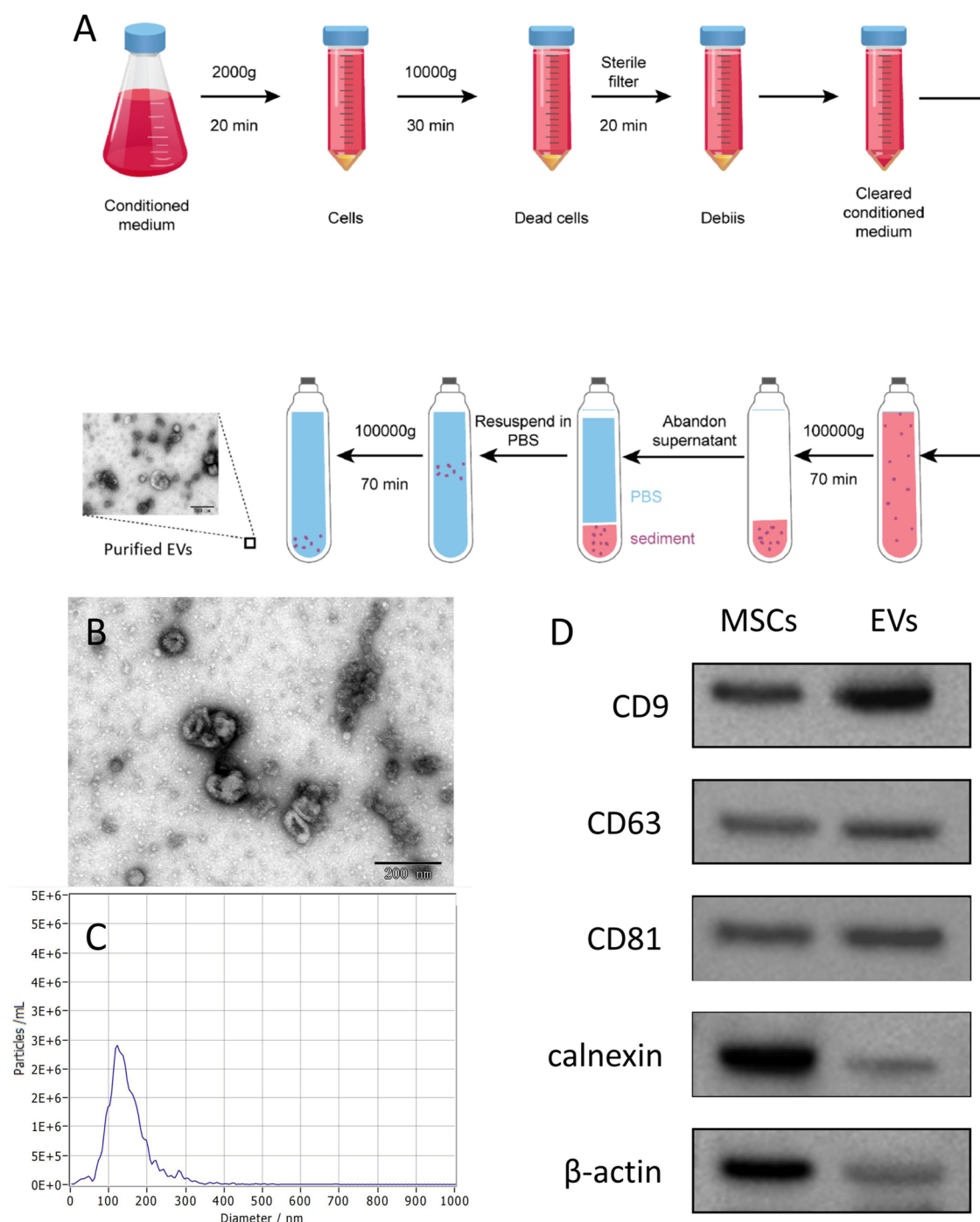
Figure 3. Isolation and characterization of EVs. (A) The process of extracting extracellular vesicles using the differential centrifugation method. (B) Morphology of extracellular vesicles under TEM (bar:200 nm). (C) Particle size distribution of EVs in NTA testing. (D) Protein expression of CD9, CD63, CD81, and calnexin in Western blot analysis.

washing with TBST and were then treated with a developing solution. This was followed by chemiluminescent imaging.

RESULTS AND DISCUSSION

Preparation and Characterization of the DMAEMA-*b*-THPMA Micelles. Using a poly(*N,N′* dimethylacrylamide) chain transfer agent conjugate and tetrahydropyranyl methacrylate monomer in the initiator reaction conditions, a poly(*N,N′* dimethylacrylamide-*b*-tetrahydropyranyl methacrylate) block copolymer was obtained. The DMAEMA-*b*-THPMA polymer with a putamer-core structure with a hydrophobic bond segment inside and a hydrophilic bond segment outside was successfully synthesized by sequential RAFT polymerization (Figure 1B). The synthesized micelles exhibited a liquid morphology and the Dingdall phenomenon (Figure 2A). The successful synthesis of the DMAEMA-*b*-THPMA polymer was confirmed through proton nuclear magnetic resonance spectroscopy (Figure 2B). The NMR spectra of the DMAEMA-*b*-THPMA polymer following ultrasound treatment are depicted in Figure 2C. The results of gel permeation chromatography (GPC) are summarized as
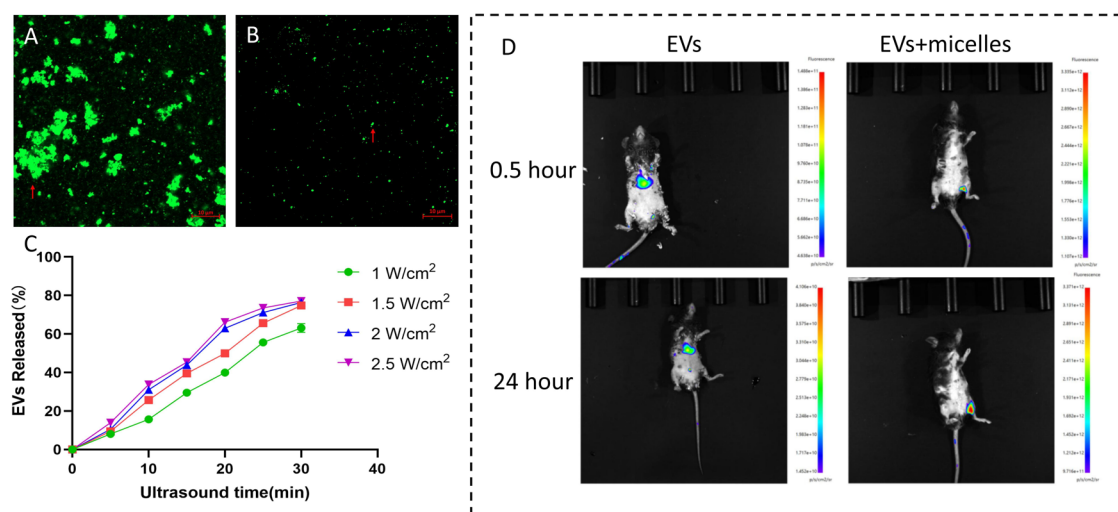
Figure 4. EVs release from DMAEMA-*b*-THPMA micelles. (A) Fluorescence image of EVs-loaded micelles. (B) Fluorescence image of EVs released after ultrasound. (C) Release profiles of EVs from micelles under different ultrasound conditions (*n* = 3). (D) (db/db) mice received a tail intravenous injection of DiR-stained EVs or EVs-loaded micelles. *In vivo* imaging techniques were used for the visualization of the spatial distribution of EVs labeled with fluorescent markers within an organism. In the EVs group, fluorescently labeled EVs exhibited a predominant distribution within the thoracic cavity and kidney region. In the EVs+micelle group, the distribution of fluorescently labeled EVs was predominantly observed in the lower extremities following ultrasound treatment.

follows: Mn = 14617 g/mol; MW theory = 20699 g/mol; and PDI = 1.49.

Transmission electron microscopy was used to observe the morphology and size of the micelles prior to and after the addition of EVs, as shown in Figure 2D,E. The DMAEMA-*b*-THPMA micelles appear as regular round spheres under phosphotungstic acid staining. The EVs-loaded micelles also appeared as regular spheres, but the diameter was larger than that before loading. It can be seen that the DMAEMA-*b*-THPMA micelles before and after EVs loading can have a certain stability in PBS solution (pH 7.4). Moreover, the diameter of the whole system increased after the EVs were loaded. These results were also confirmed by the dynamic light scattering (DLS) method (Figure 2F). According to the DLS data, the diameter of the blank micelles was 75.5 nm. However, the micelle diameter decreased to 6.8 nm after sonication. Additionally, the DMAEMA-*b*-THPMA micelles underwent morphological changes in response to ultrasound. Based on the results described above, The dynamic diameter of the drug-loaded micelles increased compared to before drug. This result aligns with the research findings of Professor Cao.[39] In comparison to blank micelles, the loaded micellar system exhibits no alteration in the inherent properties of the micelles but demonstrates an increase in their diameter in the micellar state. Under the influence of ultrasound, the micelle diameter undergoes a significant reduction. This outcome can be attributed to the ultrasonic-induced deaggregation of the micellar system, resulting in its overall collapse. These findings substantiate that micelles exhibit a responsiveness to ultrasound for controlled release.

Selecting a drug delivery system that can encapsulate EVs is of utmost importance and must account for factors such as biocompatibility, nanoscale architecture, and targeted release capability. The requirements mentioned above can be fulfilled by stimulus-responsive polymers. Stimulated-sensitive polymers possess distinct functional groups, allowing them to display customized reactions to slight variations in nearby physical or chemical conditions, ultimately leading to

modifications in their material composition and characteristics. Several studies have utilized the acidic conditions of the tumor microenvironment as a stimulus for the controlled release of chemotherapeutic agents encapsulated within block copolymers.[40] Furthermore, there have been additional investigations that utilized red light stimulation to induce the liberation of medications from obstruct polymers.[41] However, targeted delivery to microcirculation lesions is not suitable under the stimulation conditions. Microcirculation lesions lack specifically acidic environments such as those found in tumor microenvironments, and while photodynamic therapy can inhibit tumor cell growth, it does not promote endothelial cell regeneration in microcirculation lesions. Low-energy-density ultrasound is a low-intensity form of mechanical energy that minimizes thermal damage to the body while ensuring efficient transmission of acoustic energy to the target tissue.[42] Some studies[43] have demonstrated that low-energy ultrasound can enhance intracellular nitric oxide (NO) synthase activity and upregulate VEGF gene expression by elevating NO levels, thereby promoting angiogenesis. It has been suggested that the advantageous impacts of low-power ultrasound are achieved by activating the crucial PI3K/Akt signaling pathway, thereby promoting angiogenesis.[44] Ultrasound-responsive micelles, as self-assembled block copolymers, exhibit excellent biocompatibility and structural stability. Multiple studies have confirmed the ability of ultrasound-responsive micelles to execute precise drug release under low-energy-density ultrasound stimulation.[45] Hence, this study successfully achieved the intended objective of targeted release of EVs in microcirculatory lesions by utilizing low-power ultrasound as a stimulation condition.

Preparation and Characterization of EVs. The HUCMSCs were verified by a three-lineage differentiation assay and flow cytometry analysis (Figure S1).[46] In the culture medium, EVs secreted from HUCMSCs were isolated by differential centrifugation (Figure 3A). TEM and NTA were utilized to ascertain the structure and dimensions of the EVs. EVs structures were observed by TEM to be cup-shaped double capsules. The particle size of the EVs was
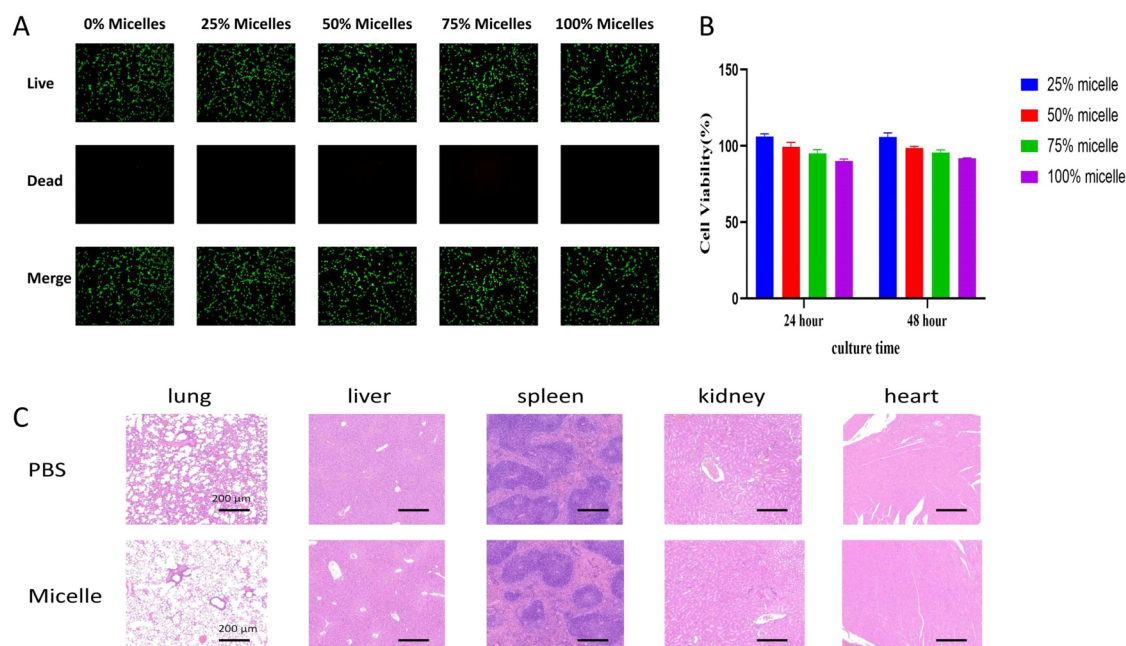
Figure 5. Biocompatibility and biosafety analysis. (A) Fluorescence plots of live and dead cells stained in different concentrations of micelles(n = 3). (B) Cell viability against different concentrations of micelles (n = 3). (C) Histology examination of tissue sections of vital organs after micelle injection (bar: 200 μm).

approximately 100 nm according to TEM (Figure 3B). The NTA data (Figure 3C) showed that the EVs dimensions varied between 100 and 140 nm, which corresponded to the TEM images. The expression of EVs-specific markers (CD9, CD63, and CD81) and an endoplasmic reticulum membrane marker (calnexin) was observed in the Western blot analysis (Figure 3D). The above results indicate that EVs were successfully extracted from HUCMSCs with high purity.

EVs Release from the DMAEMA-b-THPMA Micelles. DMAEMA-b-THPMA micelles can be used for targeted drug release by ultrasound. Figure 1A illustrates how this characteristic could potentially facilitate the utilization of EVs for the management of microcirculation disorders, leading to a decrease in the needed EVs dosage and minimizing their effects on nontargeted areas. To assess the capability of micelles to release medications using ultrasound, both *in vitro* and *in vivo* experiments were conducted. In the experiment conducted in a controlled environment (Figure 4A,B), the EVs stained with DiO underwent a transformation following sonication. They transitioned from being encapsulated and clustered by micelles to liberating and scattered. To determine the release effect on EVs of different energy densities and different ultrasound durations, experiments regarding *in vitro* cell release were performed at different time points (range: 5−30 min) and different energy densities (0.5−2.0 W/cm2). The study was conducted in a simulated physiological environment resembling that of a human (PBS, pH 7.4, 37 °C). The experimental results are listed in Figure 4C. As the energy density and time of ultrasound increased, more

EVs were released from the micelles. The release rate of the EVs was close to the peak after 30 min of sonication, and the amount of EVs released was close to 80% of the total number in the micelles. During the *in vitro* study conducted in a simulated physiological setting, the DMAEMA-b-THPMA micelles demonstrated efficient EVs release when exposed to ultrasound. During the *in vivo* study, the micelles containing

EVs also exhibited favorable localized drug release (Figure 4D). DiR-stained EVs were observed to accumulate in the heart and kidneys of mice injected only with EVs. In mice injected with EVs-loaded micelles and treated with ultrasound, EVs were mainly localized to the lower limbs. The above experiments showed that the EVs loaded in the DMAEMA-b-THPMA micelles could be targeted and released under the action of ultrasound.

Biocompatibility and Biosafety Testing. The detection of biotoxicity is very important for the application of materials in biomedical fields.[47] Different concentrations (25, 50, 75, and 100%) of micelles were used to culture HUVECs. The effect of different micelle concentrations on cellular function was evaluated through the CCK-8 test and the staining of live and dead cells. Figure 5A,B shows that cells cultured with low concentrations (25%) of micelles showed a slight increase in cell viability. This phenomenon may have occurred because the micelles made the cells more adherent, thus allowing the cells to proliferate faster. However, cell proliferation was slightly inhibited when cells were cultured with a high concentration (100%) of micelles. This may be related to the excess micelles occupying the growth space of the cells as well as the reduced

volume of medium. Overall, the rate of cell growth remained consistently above 90% throughout the cell culture process, regardless of the varying concentrations of micelles used. The findings suggest that gelatin micelles do not exhibit any apparent harmful impact on human umbilical vein endothelial cells. No apparent abnormalities were observed in the heart, liver, spleen, lung, or kidney of mice administered micelles or mice administered PBS during the *in vivo* experiments (Figure 5C). The results from the *in vivo* tests were basically in agreement with those acquired from the *in vitro* tests.

Impact of EVs on Vascular Cells. To elucidate the efficacy of EVs in treating lower extremity microcirculation lesions, we initially conducted *in vitro* experiments utilizing EVs on endothelial cells. In the confocal fluorescence
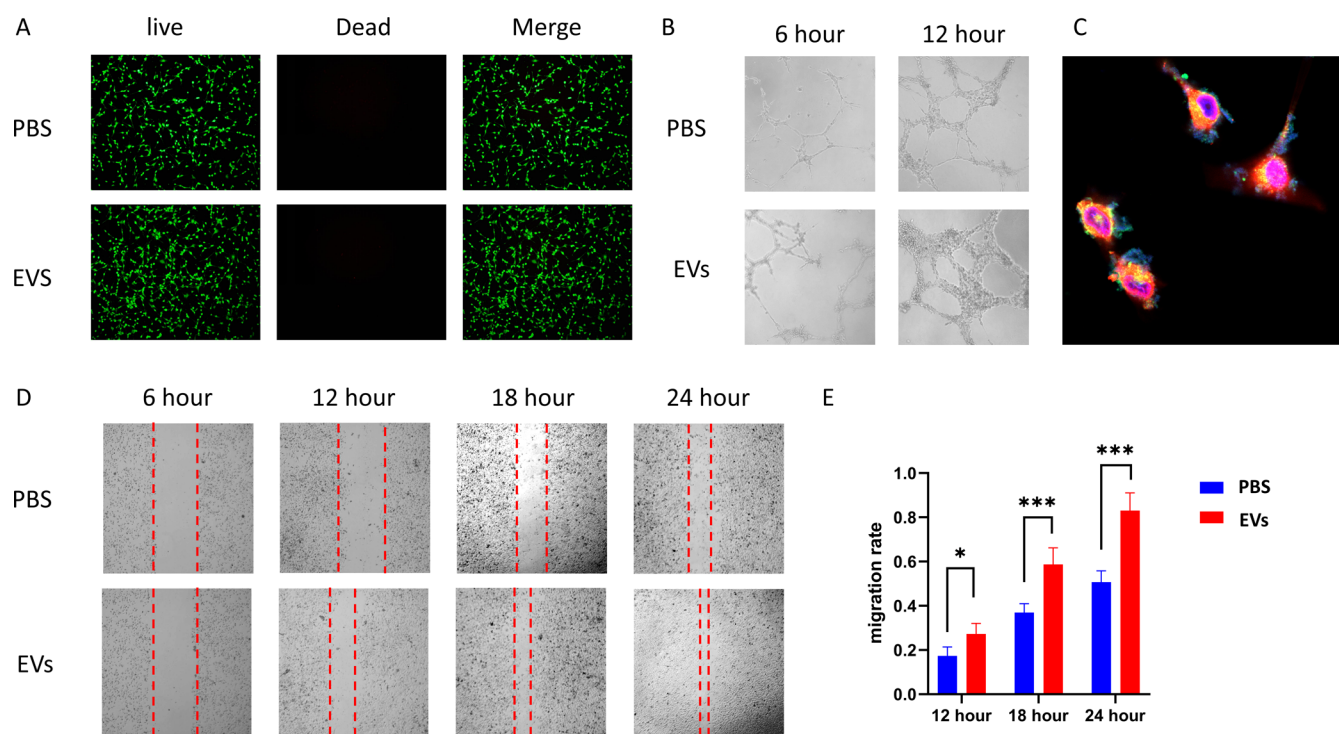
Figure 6. Effect of EVs on endothelial cells. (A) Fluorescence plots of live and dead cells stained in the EVs and PBS groups ($n = 3$). (B) Tube length and number of branches in HUVECs cocultured with EVs or PBS by tube formation assay ($n = 3$). (C) Uptake of EVs by endothelial cells. Combining confocal images with DiO-labeled EVs (green), DAPI (blue) stained nuclei, and TRITC (red) stained cytoplasm. (D, E) Cell scratch test was used to detect the effect of EVs on the migration ability of endothelial cells ($n = 3$, mean $\pm$ SD, *$p < 0.05$, ***$p < 0.001$).

microscopy images (Figure 6C), the HUVECs were immunostained with phalloidin-TRITC (red) and DAPI (blue). The EVs were immunostained with DiO (green). After 24 h of coculture, the majority of EVs were observed to be in both the nucleus and cytoplasm, indicating that endothelial cells possess a robust capacity for EVs uptake. By employing live/dead cell staining and CCK-8 assay analysis, we noticed a considerably enhanced cellular proliferation rate in the EVs group when compared to the PBS group (Figure 6A). To evaluate the effect of EVs on the angiogenic capability of endothelial cells, a tube formation test was employed (Figure 6B). In comparison to the control group, the EVs group exhibited a notably greater quantity of tubules and tubule junctions generated by HUVECs. HUVECs cultured in Matrigel were stimulated to form tubules in the presence of EVs. The migration of HUVECs was induced by EVs in the cell migration assay after a 12−24 h period (Figure 6D). The migration rate was ascertained through computation of the proportion of cells between the farthest point from its starting position and the overall distance traveled (Figure 6E). The EVs group exhibited a greater migration distance and migration rate than those of the PBS group. The findings indicate that endothelial cells can effectively internalize EVs. Furthermore, EVs can enhance the growth, tubulogenesis, and movement of endothelial cells.

The prevalence of lower limb ischemia is high among patients with peripheral vascular diseases with microcirculation lesions posing significant challenges to its management. The pathogenesis of microcirculation lesions primarily involves the suppression of angiogenesis, inflammation, and infection.[48] With recent progress in cellular technology, stem cells have become a promising and potential treatment option for regenerative medicine. Specifically, mesenchymal stem cells

(MSCs) have shown considerable therapeutic promise in addressing lower limb ischemia.[49] Nevertheless, the practical implementation of MSC treatment continues to encounter various obstacles, such as the potential for tumor formation and ethical considerations.[50] Moreover, the effectiveness of stem cells in addressing microcirculation injuries is impeded by their small cellular size. EVs are small, round extracellular vesicles that vary in diameter from 40 to 150 nm. Cells release them into bodily fluids, which consist of different genetic materials, lipids, and proteins. Through the transfer of these bodies between cells, EVs can induce corresponding cellular biological effects.[51] EVs secreted by MSCs containing cytokines and genetic material have the ability to regulate cell proliferation, exhibit anti-inflammatory effects, and promote angiogenesis. In a murine model of diabetic lower limb ischemia, Wang and colleagues[52] found that the JAK/STAT6 pathway is influenced by EVs adipose-derived from derived stem cells, leading to the modulation of macrophage polarization. These findings suggest a potential therapeutic application with a promising efficacy. In their study, Zhang and colleagues showed that EVs obtained from stem cells derived from adipose tissue have a beneficial impact on endothelial cells and stimulate the formation of new blood vessels in diabetic mice suffering from lower limb ischemia.[53] This study showcased the capability of EVs obtained from MSCs to augment the proliferation and migration of endothelial cells as well as facilitate the formation and restoration of blood vessels, both in laboratory settings and living organisms. To some degree, control of blood sugar levels also contributes to the management of microvascular complications. The results indicate that EVs derived from MSCs show significant potential for treating ischemic diseases of the lower limbs (Figure 7).
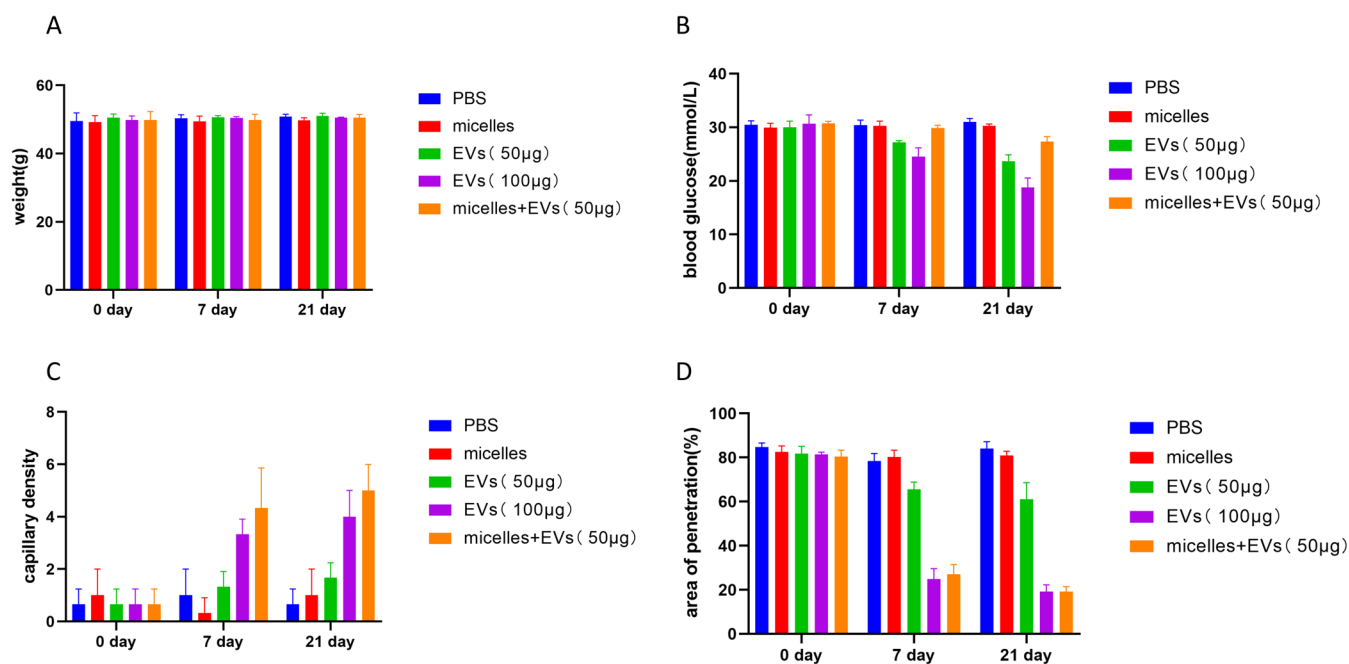
Figure 7. (A) Comparison of the weight in each group of mice on day 0, day 7, and day 21 ($n = 3$). (B) Comparison of blood glucose levels in each group of mice on 0, 7, and 21 days ($n = 3$). (C) Comparison of the number of capillaries under each high-power microscope in each group ($n = 3$). (D) Comparison of the proportion of muscle tissue stained with EB dye infiltrated by each group ($n = 3$).
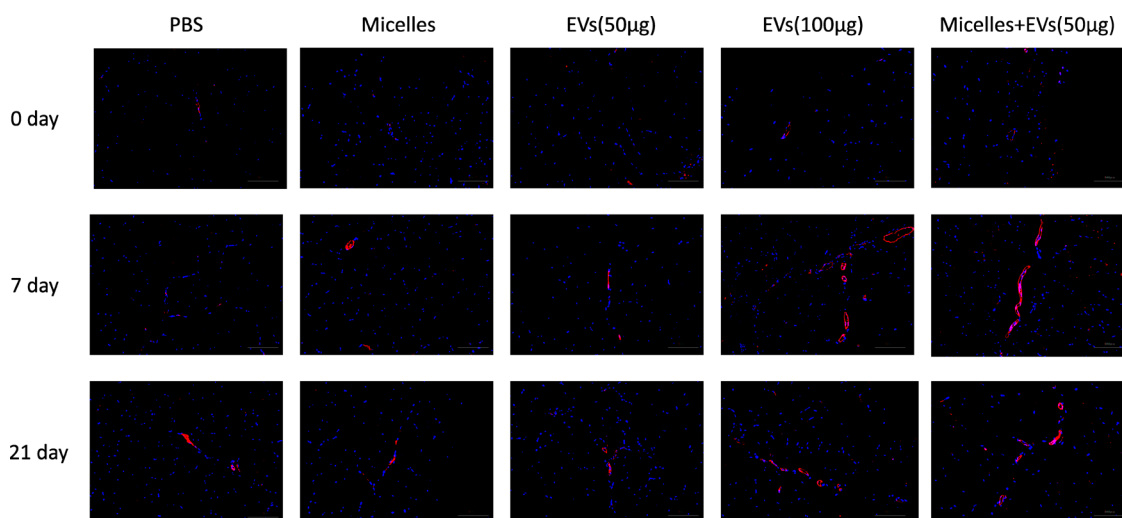

Figure 8. Immunofluorescence staining for the evaluation of vascularity in different groups. The expression of CD31 was confirmed by double staining with CD31 (red) and DAPI (blue) on vascular endothelial cells (bar:100 μm).

***In Vivo* Therapeutic Effects and Potential Mechanisms of EVs-Loaded Micelles.** To examine the healing properties of micelles in living organisms, we categorized the mice into five groups: PBS, micelles, EVs (50 μg), EVs (100 μg), and a mixture of micelles and EVs (50 μg). Body weight, blood glucose levels, microvessel density, microvessel permeability, and microvessel morphology were assessed at specified time points in each group of mice. We assessed neovascularization growth in each group through CD31 immunofluorescence staining with vascular endothelial cells appearing red. In Figure 8, the EVs-loaded micelle group showed the greatest number of blood vessels marked with red fluorescence in comparison to the remaining groups, with the EVs group coming next. Injecting a high dose of EVs and the targeted release of EVs encapsulated in micelles both exerted

significant impact on promoting microvascular angiogenesis. The promotion of vascular generation by injecting a low dose of EVs was also observed to some extent, albeit not as pronounced as those of the aforementioned two groups. Microvascular permeability was evaluated by using EB perfusion. Figure 9 clearly shows that the extravasation of EB dye was significantly reduced in both the EVs (100 μg) group and the group treated with EVs-loaded micelles. The findings suggest that EVs have the potential to effectively attenuate microcirculatory permeability in muscle tissue. Using an electron microscope (Figure 10), we examined the morphological formation of microvessels in every group. The vascular structure in the PBS, micelle, and EVs (50 μg) groups showed constricted lumens, with endothelial cells exhibiting fingerlike projections and an elevated number of endocytic vesicles.
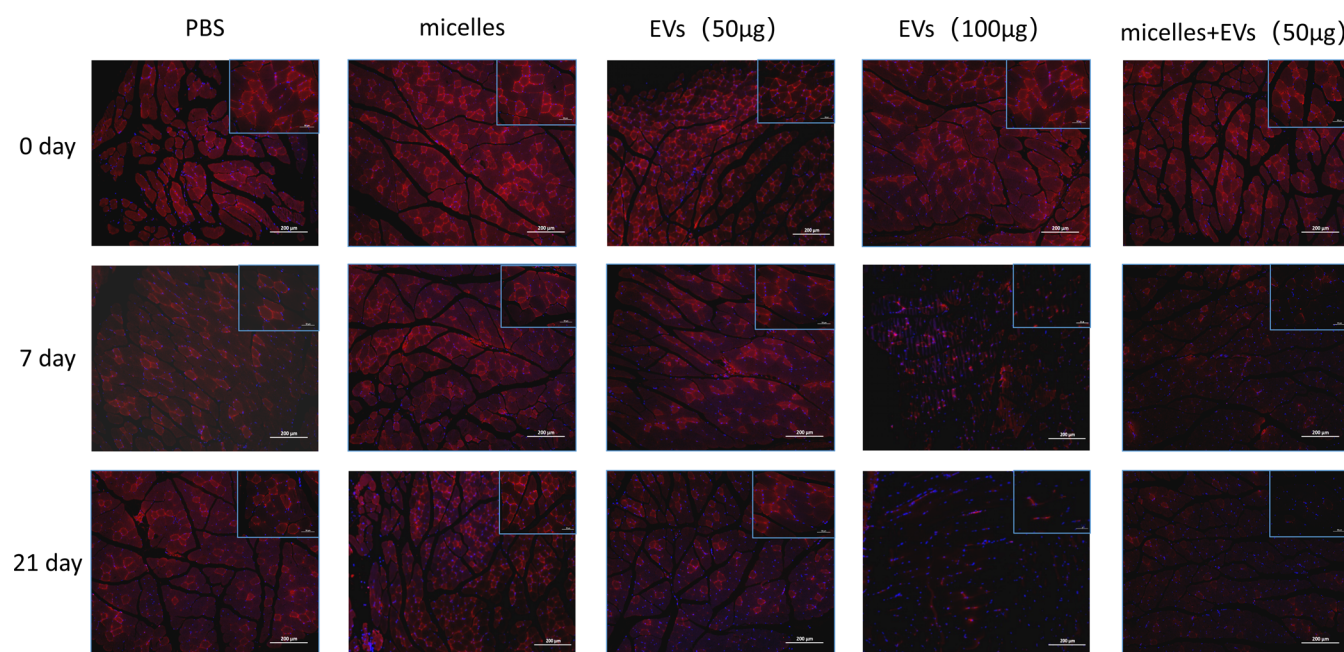
Figure 9. Evans blue perfusion method used to detect the permeability of microvessels in the lower limbs. The red color represents the extravasated Evans blue dye. The blue color indicates muscle tissue labeled with DAPI (bar: 200 μm).
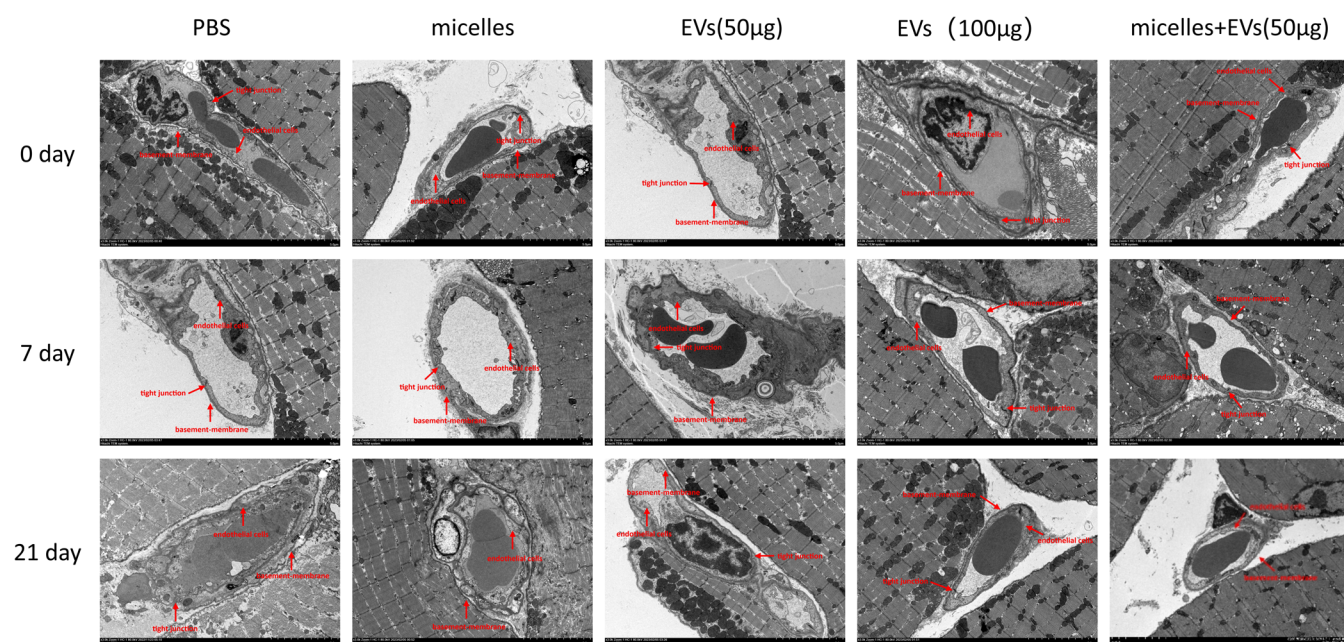

Figure 10. Visualization of the capillary ultrastructure through electron microscopy. In the EVs (100 μg) group and the micelle+EVs (50 μg) group, the lumen of the microvessels was smooth, with a smooth and intact surface of endothelial cells and normal intercellular gaps between endothelial cells. In the other groups, the lumen of the microvessels was narrow, with disruption of luminal integrity and widening of intercellular gaps in endothelial cells.

Additionally, mitochondrial swelling, vacuolar degeneration, and disruption of integrity were observed, along with widened gaps between endothelial cells. Nevertheless, in both the EVs (100 μg) group and the group treated with EVs-loaded micelles, the microvascular lumen exhibited a sleek appearance, with endothelial cell surfaces remaining intact and intercellular spaces appearing normal. In conclusion, a high dose (100 μg) of EVs promoted neovascularization while improving the vascular permeability and repairing vascular damage. Although low doses of EVs also exhibited therapeutic effects, these

effects were not significant. Figure 11 illustrates the crucial involvement of Bax, Bcl-2, and vegf-α in angiogenesis at the protein level. To examine whether the EVs treatment of microcirculation lesions is linked to these proteins, Western blot analysis was performed to evaluate their levels of expression. According to the illustration, EVs treatment resulted in increased levels of vegf-α (a promoter of angiogenesis) and Bcl-2 (a suppressor of apoptosis) in each of the three groups, with the micelle group displaying the most elevated expression. Conversely, a contrasting trend was
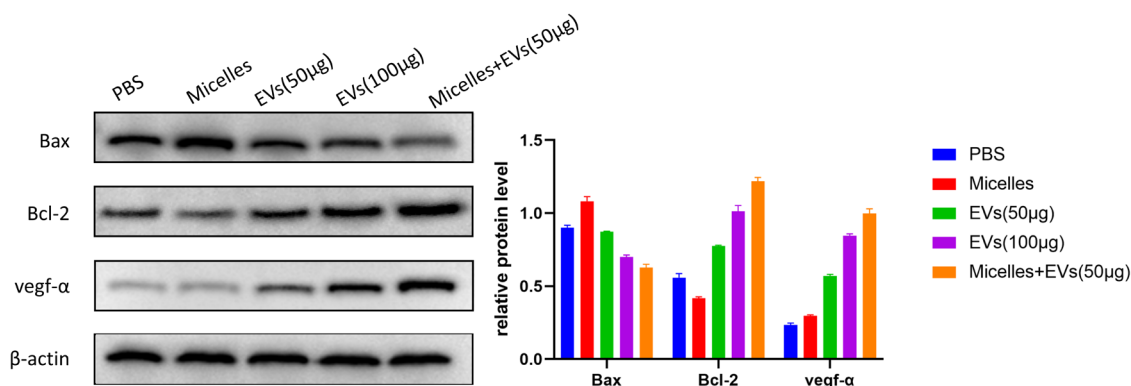
Figure 11. Expression of promoting angiogenesis-related proteins of the five groups by Western blot analysis. β-Actin protein was used as the internal reference protein.

observed for Bax (associated with apoptosis). In general, when administered at a reduced dosage, EVs-loaded micelles promoted the release of vegf-α and Bcl-2 while inhibiting the manifestation of Bax.

EVs experience a considerable decrease in transportation efficiency when employed for the therapy of lower extremity ischemic disorders. After injection, EVs predominantly accumulate in the heart and kidney, with only a minor fraction exerting their effects on microcirculation lesions.[54] The emergence of nanotechnology and the advent of "precision therapy" have propelled targeted nanomedicine to the forefront of drug research.[55] The group of mice with the highest EVs content in our experiments exhibited the most significant effect on reduced blood glucose levels (Figure 7B), possibly due to the localized release of micelle-encapsulated EVs resulting in a reduced number of EVs acting on the liver and pancreas.

Both the high-dose EVs group and the group with EVs encapsulated in micelles exhibited beneficial therapeutic effects in the microcirculation lesion model. A comparison was made between the groups regarding the alterations in body weight and blood glucose levels. Despite the absence of notable weight alteration in the mice across all groups following the intervention, a distinct reduction in blood glucose levels was apparent, particularly in the mice administered with EVs (Figure 7A,B). This observation suggests a potential role for the glucose-regulating properties of EVs derived from MSCs, as reported in previous studies. Anti-CD31, as a specific antibody for endothelial cells labeled with a fluorescent dye, clearly shows the microvessel density and allows for the evaluation of angiogenic potential.[56] The study observed varying levels of pro-angiogenic effects among the groups that received EVs. Research has shown that severe ischemia may cause the breakdown of microvascular formations, resulting in a notable rise in microvascular exudation.[57] The permeability of microvessels in the lower limbs was assessed by using EB perfusion, while structural changes in microvessels were observed through electron microscopy. The findings revealed that both the high-dose EVs group and the EVs-loaded micelle group exhibited relatively intact microvascular structures with low permeability. Similarly, the low-dose EVs group demonstrated comparable results. Conversely, significant damage to microvascular structures and substantial extravasation were observed in the other groups. From these observations, it is evident that ultrasound-responsive micelles exhibit superior capabilities in vascular regeneration and repair, even with a

reduced EVs dosage. This outcome may be attributed to the enhanced delivery of EVs to the injury site and the angiogenic stimulation induced by low-energy density ultrasound. Some studies have examined the capability of ultrasound-triggered micelles to release enclosed substances.

■ CONCLUSIONS

For the treatment of microcirculation diseases in the lower extremities, a new method of drug delivery using EVs encapsulation was utilized in this research. The DMAEMA-b-THPMA polymer was synthesized via RAFT from the THPMA and DMAEMA monomers. Under the influence of ultrasound, well-prepared micelles can be selectively released at a particular location, inside or outside a living organism in a laboratory setting. The safety of the micelles in endothelial cells and mice was confirmed through biocompatibility experiments. Endothelial cell proliferation, migration, and angiogenesis were assessed through *in vitro* cell experiments. *In vivo* animal experiments demonstrated that the EVs-loaded micelle system had satisfactory therapeutic effects on lower limb ischemia model animals. This study suggests that ultrasound-responsive micelles have great potential as targeted drug-loading systems when combined with MSC-derived EVs, resulting in a "1 + 1 > 2" effect.

■ ASSOCIATED CONTENT

■ AUTHOR INFORMATION

Corresponding Author
  Bing Wang − *The Fifth Affiliated Hospital of Zhengzhou University, Zhengzhou 450001 Henan, China;* Email: hnxgwk@126.com

Authors
  Peng Guo − *The Fifth Affiliated Hospital of Zhengzhou University, Zhengzhou 450001 Henan, China;* ⓞ orcid.org/0009-0002-2573-9920
  Qian Wang − *College of Materials and Chemical Engineering, West Anhui University, Luan 237012 Anhui, China*
  Ling Chen − *The First Affiliated Hospital of Lanzhou University, Lanzhou 730000 Gansu, China*

Kun Dingya − *The Fifth Affiliated Hospital of Zhengzhou University, Zhengzhou 450001 Henan, China*

Complete contact information is available at:
https://pubs.acs.org/10.1021/acsomega.3c08133

Author Contributions

P.G.: Manipulation of most of the experiments in the study and manuscript writing. Q.W.: Synthesis of chemical materials experiments, the operation of material experiments, and the sharing of chemical materials knowledge. (1) C.L.: Help to complete some medical experiments and provide some experimental funding support. (2) Y.D.: Help to complete some medical experiments and discuss research topics. (3) B.W.: Complete the design of the whole experiment and provide some experimental funding support

Notes

The authors declare no competing financial interest.

■ REFERENCES

(1) Wawruch, M.; Wimmer, G.; Murin, J.; et al. Non-Adherence to Statin Treatment in Older Patients With Peripheral Arterial Disease Depending on Persistence Status. *J. Vasc. Surg.* **2021**, *73* (1), 344.

(2) Oh, S.; Son, M.; Park, C. H.; et al. Pyrogallol-Phloroglucinol-6,6-Bieckolon Attenuates Vascular Smooth Muscle Cell Proliferation and Phenotype Switching in Hyperlipidemia through Modulation of Chemokine Receptor 5. *Drugs* **2020**, *18* (8), 393.

(3) Bradbury, A. W.; Moakes, C. A.; Popplewell, M.; et al. A vein bypass first versus a best endovascular treatment first revascularisation strategy for patients with chronic limb threatening ischaemia who required an infra-popliteal, with or without an additional more proximal infra-inguinal revascularisation procedure to restore limb perfusion (BASIL-2): an open-label, randomised, multicentre, phase 3 trial. *Lancet* **2023**, *401*, 1798−1809.

(4) Gerhard-Herman, M. D.; Gornik, H. L.; Barrett, C.; et al. 2016 AHA/ACC Guideline on the Management of Patients With Lower Extremity Peripheral Artery Disease: A Report of the American College of Cardiology/American Heart Association Task Force on Clinical Practice Guidelines. *J. Am. Coll Cardiol* **2017**, *69*, e71−e126.

(5) Barker, R. A.; Parmar, M.; Studer, L.; et al. Human Trials of Stem Cell-Derived Dopamine Neurons for Parkinson's Disease: Dawn of a New Era. *Cell Stem Cell* **2017**, *21*, 569−573.

(6) Rigato, M.; Monami, M.; Fadini, G. P. Autologous cell therapy for peripheral arterial disease: systematic review and meta-analysis of randomized, non-randomized, and non-controlled. *Circ. Res.* **2017**, *120* (8), 1326−1340.

(7) Cosson, S.; Otte, E. A.; Hezaveh, H.; et al. Concise Review: Tailoring Bioengineered Scaffolds for Stem Cell Applications in Tissue Engineering and Regenerative Medicine. *Stem Cells Transl. Med.* **2015**, *4* (2), 156−164.

(8) Liu, J.; Qiu, P.; Qin, J.; et al. Allogeneic adipose-derived stem cells promote ischemic muscle repair by inducing M2 macrophage polarization via the HIF-1α/IL-10 pathway. *Stem Cells* **2020**, *38*, 1307−1320.

(9) Chen, Y.; Huang, H.; Li, G.; et al. Dental-derived mesenchymal stem cell sheets: a prospective tissue engineering for regenerative medicine. *Stem Cell Res. Ther.* **2022**, *13* (1), No. 38.

(10) Wang, Y.; Huang, J.; Gong, L.; et al. The Plasticity of Mesenchymal Stem Cells in Regulating Surface HLA-I. *iScience* **2019**, *15*, 66−78.

(11) Huang, W.; Lin, M.; Yang, C.; et al. Rat Bone Mesenchymal Stem Cell-Derived Exosomes Loaded with miR-494 Promoting Neurofilament Regeneration and Behavioral Function Recovery after Spinal Cord Injury. *Oxid Med. Cell Longev.* **2021**, No. 1634917.

(12) Wang, Yi.; Ma, Xibo.; Chai, Wei.; et al. Multiscale Stem Cell Technologies for Osteonecrosis of the Femoral Head. *Stem Cells Int.* **2019**, *2019*, No. 8914569.

(13) Park, J. J.; Kwon, Y. W.; Kim, J. W.; et al. Coadministration of endothelial and smooth muscle cells derived from human induced pluripotent stem cells as a therapy for critical limb ischemia. *Stem Cells Transl. Med.* **2021**, *10*, 414−426.

(14) Heo, J.; Kang, H. Exosome-Based Treatment for Atherosclerosis. *Int. J. Mol. Sci.* **2022**, *23* (2), No. 1002, DOI: 10.3390/ijms23021002.

(15) Bocheng, Z.; Xiaoyuan, T.; Zhenan, Q.; et al. Hypoxia-Preconditioned Extracellular Vesicles from Mesenchymal Stem Cells Improve Cartilage Repair in Osteoarthritis. *Membranes* **2022**, *12* (2), No. 225.

(16) Bellavia, D.; Raimondi, L.; Costa, V.; et al. Engineered exosomes: A new promise for the management of musculoskeletal diseases. *Biochim. Biophys. Acta, Gen. Subj.* **2018**, *1862*, 1893−1901.

(17) Anderson, J. D.; Johansson, H. J.; Graham, C. S.; et al. Comprehensive Proteomic Analysis of Mesenchymal Stem Cell exosomes Reveals Modulation of Angiogenesis via Nuclear Factor-KappaB Signaling. *Stem Cells* **2016**, *34*, 601−613.

(18) Wang, C.; Liang, C.; Wang, R.; et al. The fabrication of a highly efficient self-healing hydrogel from natural biopolymers loaded with exosomes for the synergistic promotion of severe wound healing. *Biomater. Sci.* **2019**, *8*, 313−324.

(19) Antimisiaris, S. G.; Mourtas, S.; Marazioti, A. Exosomes and exosome-Inspired Vesicles for Targeted Drug Delivery. *Pharmaceutics* **2018**, *10* (4), No. 218, DOI: 10.3390/pharmaceutics10040218.

(20) Li, Z.; Gupta, M. K.; Barajas, M. B.; et al. Newly Developed Di-Block Copolymer-Based Cell Membrane Stabilizers Protect Mouse Coronary Artery Endothelial Cells against Hypoxia/Reoxygenation Injury. *Cells* **2023**, *12* (10), No. 1394.

(21) Ramirez, D. G.; Abenojar, E.; Hernandez, C.; et al. Contrast-enhanced ultrasound with sub-micron sized contrast agents detects insulitis in mouse models of type1 diabetes. *Nat. Commun.* **2020**, *11*, No. 2238.

(22) Lin, S.; Zhu, L.; Li, Z.; et al. Ultrasound-responsive glycopolymer micelles for targeted dual drug delivery in cancer therapy. *Biomater Sci.* **2023**, *11*, 6149−6159.

(23) Elladiou, M.; Patrickios, C. S. ABC Triblock Terpolymers with Orthogonally Deprotectable Blocks: Synthesis, Characterization, and Deprotection. *Macromolecules* **2015**, *48*, 7503−7512.

(24) Pafiti, K. S.; Philippou, Z.; Loizou, E.; et al. End-Linked Poly[2-(dimethylamino)ethyl Methacrylate]−Poly(methacrylic acid) Polyampholyte Conetworks: Synthesis by Sequential RAFT Polymerization and Swelling and SANS Characterization. *Macromolecules* **2011**, *44* (13), 5352−5362.

(25) Thomi, G.; Surbek, D.; Haesler, V.; et al. Exosomes derived from umbilical cord mesenchymal stem cells reduce microglia-mediated neuroinflammation in perinatal brain injury. *Stem Cell Res. Ther.* **2019**, *10*, 105.

(26) Haque, S.; Vaiselbuh, S. R. Silencing of Exosomal miR-181a Reverses Pediatric Acute Lymphocytic Leukemia Cell Proliferation. *Pharmaceuticals* **2020**, *13* (9), 241.

(27) Purvis, I. J.; Velpula, K. K.; Guda, M. R.; Nguyen, D.; Tsung, A. J.; Asuthkar, S. B7-H3 in Medulloblastoma-Derived Exosomes; A Novel Tumorigenic Role. *Int. J. Mol. Sci.* **2020**, *21* (19), No. 7050.

(28) Li, Z.; Li, Q.; Tong, K.; Zhu, J.; Wang, H.; Chen, B.; Chen, L. BMSC-derived exosomes promote tendon-bone healing after anterior cruciate ligament reconstruction by regulating M1/M2 macrophage polarization in rats. *Stem Cell Res. Ther.* **2022**, *13* (1), No. 295.

(29) Bellavia, D.; Raimondo, S.; Calabrese, G.; Forte, S.; Cristaldi, M.; Patinella, A.; Memeo, L.; Manno, M.; Raccosta, S.; Diana, P.; Cirrincione, G.; Giavaresi, G.; Monteleone, F.; Fontana, S.; De Leo, G.; Alessandro, R. Interleukin 3- receptor targeted exosomes inhibit *in vitro* and *in vivo* Chronic Myelogenous Leukemia cell growth. *Theranostics* **2017**, *7* (5), 1333−1345.

(30) Zhang, L.; Wang, M.; Zhu, Z.; Ding, C.; Chen, S.; Wu, H.; Yang, Y.; Che, F.; Li, Q.; Li, H. A Novel pH-Sensitive Multifunctional DNA Nanomedicine: An Enhanced and Harmless GD2 Aptamer-Mediated Strategy for Guiding Neuroblastoma Antitumor Therapy. *Int. J. Nanomed.* 2021, *16*, 3217−3240.

(31) Gong, X.; Tang, H.; Yang, K. PER1 suppresses glycolysis and cell proliferation in oral squamous cell carcinoma via the PER1/RACK1/PI3K signaling complex. *Cell Death Dis.* 2021, *12* (3), No. 276.

(32) Shi-Cong, T.; Ting, Y.; Yue-Lei, Z.; et al. Exosomes derived from miR-140−5p-overexpressing human synovial mesenchymal stem cells enhance cartilage tissue regeneration and prevent osteoarthritis of the knee in a rat model. *Theranostics* 2017, *7* (1), 180−195.

(33) Wang, D.; Qiu, G.; Zhu, X.; et al. Macrophage-inherited exosome excise tumor immunosuppression to expedite immune-activated ferroptosis. *J. Immunother. Cancer* 2023, *11* (5), No. e006516, DOI: 10.1136/jitc-2022-006516.

(34) Sun, J.; Tang, Q.; Gao, Y.; et al. VHL mutation-mediated SALL4 overexpression promotes tumorigenesis and vascularization of clear cell renal cell carcinoma via Akt/GSK-3β signaling. *J. Exp. Clin. Cancer Res.* 2020, *39*, No. 104.

(35) Arredondo Zamarripa, David.; Noguez Imm, Ramsés.; Bautista Cortés, Ana María.; et al. Author Correction: Dual contribution of TRPV4 antagonism in the regulatory effect of vasoinhibins on blood-retinal barrier permeability: diabetic milieu makes a difference. *Sci. Rep.* 2018, *8*, No. 9652.

(36) Li, X.; Wang, Y.; Shi, L.; Li, B.; Li, J.; Wei, Z.; Lv, H.; Wu, L.; Zhang, H.; Yang, B.; Xu, X.; Jiang, J. Magnetic targeting enhances the cutaneous wound healing effects of human mesenchymal stem cell-derived iron oxide exosomes. *J. Nanobiotechnol* 2020, *18* (1), No. 113.

(37) Yamamoto, Y.; Välitalo, P. A.; Huntjens, D. R.; et al. Predicting Drug Concentration-Time Profiles in Multiple CNS Compartments Using a Comprehensive Physiologically-Based Pharmacokinetic Model. *Cpt Pharmacometrics Syst. Pharmacol.* 2017, *6* (11), 765−777, DOI: 10.1002/psp4.12250.

(38) Chen, Z.; Nie, S. D.; Qu, M. L.; et al. The autophagic degradation of Cav-1 contributes to PA-induced apoptosis and inflammation of astrocytes. *Cell Death Dis.* 2018, *9* (7), No. 771.

(39) Gannimani, R.; Walvekar, P.; Naidu, V. R.; et al. Acetal containing polymers as pH-responsive nano-drug delivery systems. *J. Controlled Release* 2020, *328*, 736−761.

(40) Cao, D.; Chen, X.; Cao, F.; et al. An Intelligent Transdermal Formulation of ALA-Loaded Copolymer Thermogel with Spontaneous Asymmetry by Using Temperature-Induced Sol−Gel Transition and Gel−Sol (Suspension) Transition on Different Sides. *Adv. Funct. Mater.* 2021, *31* (22), No. 202100349, DOI: 10.1002/adfm.202100349.

(41) Miao, Y.; Qiu, Y.; Zhang, M.; et al. Aqueous Self-Assembly of Block Copolymers to Form Manganese Oxide-Based Polymeric Vesicles for Tumor Microenvironment-Activated Drug Delivery. *Nanomicro Lett.* 2020, *12*, No. 124.

(42) Li, C.; Zhou, J.; Wu, Y.; et al. Core Role of Hydrophobic Core of Polymeric Nanomicelle in Endosomal Escape of siRNA. *Nano Lett.* 2021, *21*, 3680−3689.

(43) Sun, W.; Wen, Y.; Thiramanas, R.; et al. Red-Light-Controlled Release of Drug−Ru Complex Conjugates from Metallopolymer Micelles for Phototherapy in Hypoxic Tumor Environments.Advanced Functional Materials,. *Adv. Funct. Mater.* 2018, *28* (39), No. 1804227, DOI: 10.1002/adfm.201804227.

(44) Ren, W. W.; Xu, S. H.; Sun, L. P.; et al. Ultrasound-based drug delivery system. *Curr. Med. Chem.* 2022, *29* (8), 1342−1351.

(45) Song, L.; Lu, L.; Pu, Y.; et al. Nanomaterials-based tumor microenvironment modulation for magnifying sonodynamic therapy. *Acc. Mater. Res.* 2022, *3* (9), 971−985.

(46) Mahindran, E.; Wan Kamarul Zaman, W. S.; Ahmad Amin Noordin, K. B.; et al. Mesenchymal Stem Cell-Derived Extracellular Vesicles: Hype or Hope for Skeletal Muscle Anti-Frailty. *Int. J. Mol. Sci.* 2023, *24* (9), 7833.

(47) Li, R.; Zhou, C.; Chen, J.; et al. Synergistic osteogenic and angiogenic effects of KP and QK peptides incorporated with an injectable and self-healing hydrogel for efficient bone regeneration. *Bioact Mater.* 2022, *18* (12), 267−283.

(48) Kim, D.; Lee, A. E.; Xu, Q.; Zhang, Q.; Le, A. D. Gingiva-Derived Mesenchymal Stem Cells: Potential Application in Tissue Engineering and Regenerative Medicine - A Comprehensive Review. *Front Immunol.* 2021, *12*, No. 667221.

(49) Cossu, G.; Birchall, M.; Brown, T.; et al. Lancet Commission: Stem cells and regenerative medicine. *Lancet* 2018, *391*, 883−910.

(50) Wang, X.; Chen, S.; Lu, R.; et al. Adipose-derived stem cell-secreted exosomes enhance angiogenesis by promoting macrophage M2 polarization in type 2 diabetic mice with limb ischemia via the JAK/STAT6 pathway. *Heliyon* 2022, *8* (11), No. e11495.

(51) Poupardin, R.; Wolf, M.; Strunk, D. Adherence to minimal experimental requirements for defining extracellular vesicles and their functions. *Adv. Drug Deliv Rev.* 2021, *176*, No. 113872.

(52) Lee, Y.; El Andaloussi, S.; Wood Matthew, J. A. Exosomes and microvesicles: extracellular vesicles for genetic information transfer and gene therapy. *Hum. Mol. Genet.* 2012, *21*, R125−R134.

(53) Zhang, X.; Jiang, Y.; Huang, Q.; et al. Exosomes derived from adipose-derived stem cells overexpressing glyoxalase-1 protect endothelial cells and enhance angiogenesis in type 2 diabetic mice with limb ischemia. *Stem Cell Res. Ther* 2021, *12*, No. 403.

(54) Guo, M.; Wu, F.; Hu, G.; et al. Autologous tumor cell−derived microparticle-based targeted chemotherapy in lung cancer patients with malignant pleural effusion. *Sci. Transl. Med.* 2019, *11* (474), No. eaat5690, DOI: 10.1126/scitranslmed.aat5690.

(55) Cabral, H.; Kinoh, H.; Kataoka, K. Tumor-Targeted Nano-medicine for Immunotherapy. *Acc. Chem. Res.* 2020, *53*, 2765−2776.

(56) Xue-Lian, W.; Jia, Q.; Yi-Qin, S.; et al. Atorvastatin plus therapeutic ultrasound improve postnatal neovascularization in response to hindlimb ischemia via the PI3K-Akt pathway. *Am. J. Transl. Res.* 2019, *11*, 2877−2886.

(57) Waisman, D.; Brod, V.; Dickstein, R.; et al. Effects of inhaled nitric oxide on lung injury after intestinal ischemia-reperfusion in rats. *Shock* 2005, *23*, 150−155.